iScience

CellPress
OPEN ACCESS

Article

Shipping traffic through the Arctic Ocean: Spatial distribution, seasonal variation, and its dependence on the sea ice extent

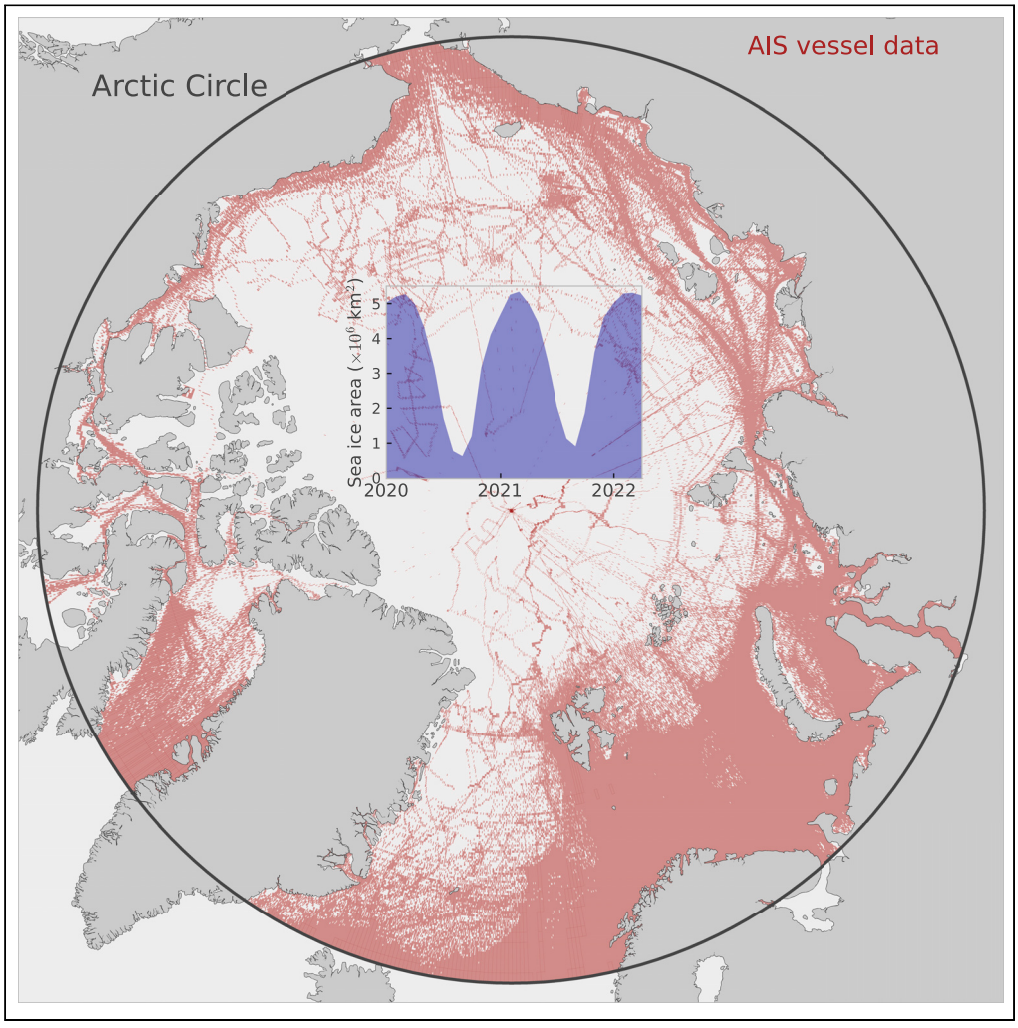

Jorge P. Rodríguez, Konstantin Klemm, Carlos M. Duarte, Víctor M. Eguíluz

jorgeprodriguezg@gmail.com

Highlights

Shipping through the Arctic Ocean is characterized by broad density distributions

The relative shipping density per longitude revealed the main shipping routes

The widths of Northeastern and Northwest Passage routes correlated with sea ice area

Rodríguez et al., iScience 27, 110236
July 19, 2024
https://doi.org/10.1016/j.isci.2024.110236

iScience

CellPress
OPEN ACCESS

Article

Shipping traffic through the Arctic Ocean: Spatial distribution, seasonal variation, and its dependence on the sea ice extent

Jorge P. Rodríguez,[1,2,3,7,*] Konstantin Klemm,[1] Carlos M. Duarte,[4] and Víctor M. Eguíluz[5,6]

SUMMARY

The reduction in sea ice cover with Arctic warming facilitates shipping through remarkably shorter shipping routes. Automatic identification system (AIS) is a powerful data source to monitor Arctic Ocean shipping. Based on the AIS data from an online platform, we quantified the spatial distribution of shipping through this area, its intensity, and the seasonal variation. Shipping was heterogeneously distributed with power-law exponents that depended on the vessel category. We contextualized the estimated exponents with the analytical distribution of a transit model in one and two dimensions. Fishing vessels had the largest spatial spread, while narrower shipping routes associated with cargo and tanker vessels had a width correlated with the sea ice area. The time evolution of these routes showed extended periods of shipping activity through the year. We used AIS data to quantify recent Arctic shipping, which brings an opportunity for shorter routes, but likely impacting the Arctic ecosystem.

INTRODUCTION

Shipping traffic represents the dominant transportation mode in global trade, delivering more than 80% of the volume of the international trade of goods.[1] In fact, economic growth has led to a parallel increase in marine traffic of 60% in the period between 1992 and 2002,[2] with projections pointing at a growth by 2050 between 240% and 1,209%, compared to 2014.[3] The importance of maritime transport to the global economy was evidenced in 2021 when the Suez Canal was blocked when the Ever Given container ship got stranded. The opportunity to leverage the opening of new Arctic routes delivering goods from Asia to Europe and North America due to the decrease of the ice cover will increase traffic and bring new threats to this vulnerable ecosystem,[4] adding to the direct impacts of rapid climate change in the Arctic. Indeed, an estimation of the shipping days per month through the Arctic Ocean has revealed an increase of 7% per year between 2013 and 2022.[5] Liquid, bulk, and general cargo transportation are currently the most important contributions to Arctic shipping,[6] while a long-term vision aims at the use of more cost-effective routes, through the Arctic Ocean, than traditional shipping routes,[7] such as the Suez Canal, Panama Canal, or Cape of Good Hope routes. According to the Intergovernmental Panel on Climate Change, any month of the year displays an Arctic ice decline in contrast to the previous records for that month, showing the strongest change in September, with a relative reduction of 12.8%.[8–10] Such decline drives projections forecasting the possibility of all-year transit by Polar Class 6 ships in the 2070s,[11] which may occur even earlier as projections have underestimated the observed patterns.[12]

Tracking technologies are playing a major role in the analysis of vessels' movement through the oceans, allowing the quantification of multiple vessel behaviors with economic, political, and ecological consequences. For example, tracking of fishing vessels facilitated the inference of hotspots of fishing activity.[13–15] Moreover, the overlap between fishing vessels' trajectories and movement tracking of marine animals has revealed regions with a high risk of overlap and thus the risk of bycatch between fishing vessels and sharks[16] and the collision risk of large vessels and bowhead whales in the Arctic.[17]

Currently, products derived from vessel tracking data are openly available. For example, Global Fishing Watch's main product describes fishing efforts at high spatial and temporal resolution globally.[13] However, broader datasets, including for instance the trajectories of other vessel categories globally, are available under private purchase. To overcome the problem of data ownership and standardization, new initiatives are being developed to perform online analyses with access to pre-filtered (i.e., spurious entries removed), pre-processed, and scientifically validated datasets from multiple sources. In this direction, HUB Ocean has developed the Ocean Data Connector (oceandata.earth), where scientists can perform online analyses of multiple datasets describing diverse oceanic phenomena, such as parasite infections in fish

[1]Instituto de Física Interdisciplinar y Sistemas Complejos (IFISC), CSIC-UIB, Palma de Mallorca 07122, Spain
[2]CA UNED Illes Balears, Palma 07009, Spain
[3]Instituto Mediterráneo de Estudios Avanzados (IMEDEA), CSIC-UIB, Esporles 07190, Spain
[4]Red Sea Research Center (RSRC), King Abdullah University of Science and Technology (KAUST), Thuwal 23955 204, Saudi Arabia
[5]Basque Centre for Climate Change (BC3), Leioa, 48940 País Vasco, Spain
[6]IKERBASQUE, Basque Foundation for Science, Bilbao, 48009 País Vasco, Spain
[7]Lead contact
*Correspondence: jorgeprodriguezg@gmail.com
https://doi.org/10.1016/j.isci.2024.110236

farms, global vessel emissions, or the geospatial data describing marine protected areas. Such platforms have the potential to track chemical, physical, biological, and economic processes in the ocean, providing valuable datasets that facilitate continuous monitoring.

Here, we report our analysis of the shipping traffic on the Arctic Ocean between January 2020 and April 2022 through a data analysis developed during a Private Preview Week of the Ocean Data Connector, providing an update of previous quantitative assessments.[18,19] We compare the empirical observations with our analytical calculations from one- and two-dimensional models of shipping transit and provide a baseline to assess the Arctic shipping time evolution, together with its correlations with sea ice extent.

RESULTS

Shipping density

The shipping density was computed as the shipping transit intensity in each grid cell divided by the cell area, aggregating the transit time from all the ships using automatic identification system in the considered region. This pattern revealed hotspots of shipping activity, both in the overall map and in the specific patterns associated with different vessel categories (Figure 1). Fishing vessels represented the largest contribution to shipping in the Arctic Ocean, especially in the Barents Sea but also in the proximity of Iceland. Cargo vessels, similarly to tanker vessels, displayed patterns where we observed the Northeastern and Northwest Passage routes. Cargo vessels' use of space became broader in the Baffin Bay, where tanker trajectories occupied less area in this region. Passenger traffic covered lower fractions of area as the most frequented routes were shorter, for example on the Norwegian and Icelandic coasts.

The shipping density heterogeneity across the space was described by heavy-tailed distributions, such that most grid cells displayed a low shipping density, with a few cells concentrating large values (Figure 2). Specifically, the shipping density distributions for the aggregated (across categories) and for specific categories were described by power-law distributions. We performed a power-law regression to these distributions with the Python package *powerlaw*, obtaining the fitted exponents 1.79 (aggregated), 1.49 (passenger), 1.90 (tanker), 1.74 (cargo), and 1.96 (fishing). For fishing, we observed two regimes, where the distribution is closer to a uniform distribution for low densities (i.e., with a smaller exponent), while large densities implied a faster decrease, which was the behavior captured by the regression.

A random null model considering an origin-destination flux, with a fixed origin and a uniform probability of reaching any destination or vice versa, leads to a uniform distribution in one dimension, while the distribution is heavy-tailed with an exponent 3 in two dimensions (see method details in STAR Methods). Fishing vessels displayed the highest exponent ($\alpha_{\text{fishing}} = 1.96$), suggesting, in parallel to the two-dimensional null model, traffic between different fishing ports and the closest fisheries. In contrast, passenger vessels showed the lowest exponent $\alpha_{\text{passenger}} = 1.49$, which we associate with more directed routes between a few ports.

Shipping routes and their temporal evolution

To detect shipping routes, we computed the average shipping density per longitude, considering only the grid cells with non-zero values, and represented the relative shipping density of each grid cell, that is, the shipping density divided by the average shipping density of its longitude (see STAR Methods). We observed that the highest values are located in the proximity of the shore (Figure 3). This technique revealed the main shipping routes (red corridors on Figure 3), as well as several fishing hotspots in the high seas. We detected two main Arctic shipping routes, the Northeastern and the Northwest Passage routes, both linking the Northern Pacific and the Northern Atlantic oceans, with the Northeastern route splitting in two at the north and south of Lyakhovsky Islands. Most of the traffic of both routes was associated with tanker and cargo vessels, as shown by the absence of spatial continuity along the routes in passenger and fishing vessels, which are expected to display shorter-range trips.

After analyzing the spatial properties of the shipping density in the aggregated dataset and across different vessel categories, we focused on the temporal evolution of the shipping traffic, aggregating all the observations across the Arctic Circle. The highest shipping traffic in the whole period corresponded to fishing vessels followed, in decreasing order, by passenger, cargo, and tanker vessels (Figure 4). While the relative evolution of fishing and passenger vessels did not display large relative fluctuations, the shipping traffic for cargo and tanker vessels showed maximum activity in the summer and early autumn of both 2020 and 2021.

Longitudinal heterogeneity: Seasonal behavior and correlations with sea ice area

To quantify the time evolution of the shipping routes that we observed in Figure 3, we computed the average shipping density and the shipping width for each meridional cross-section (that is, zones with constant longitude and varying latitude, see STAR Methods), leading to a representation of the zonal variability of these variables. First, we observed that the average shipping density, an indicator of the potential ecological impact on the transited areas, displayed a seasonal behavior in most of the longitudes except for those in the Norwegian, Greenland, and Barents seas, where the traffic was not interrupted in the analyzed period (Figure 5, top). As the relative shipping density (Figure 3) suggested that vessels displayed mainly longitudinal movement, we quantified the availability of routes and their actual use computing the time evolution across longitudes of the shipping width, observing the same seasonal behavior, and the appearance of long-range routes whose widths were maximum at the late summer and early autumn, with vessels using the Northeastern route for 4 months, while they transited the Northwest Passage route for 2–3 months (Figure 5, bottom), with these periods overlapping with the relative maxima of the shipping traffic for cargo and tanker vessels (Figure 4). This temporal evolution of the routes allowed us to select two longitudes as the most representative for the Northeastern (150°) and the Northwest Passage (−90°) routes. These longitudes displayed a null shipping density in winter, while other longitudes in the same route showed some densities that we link to local transit. We considered that the environmental variable with the

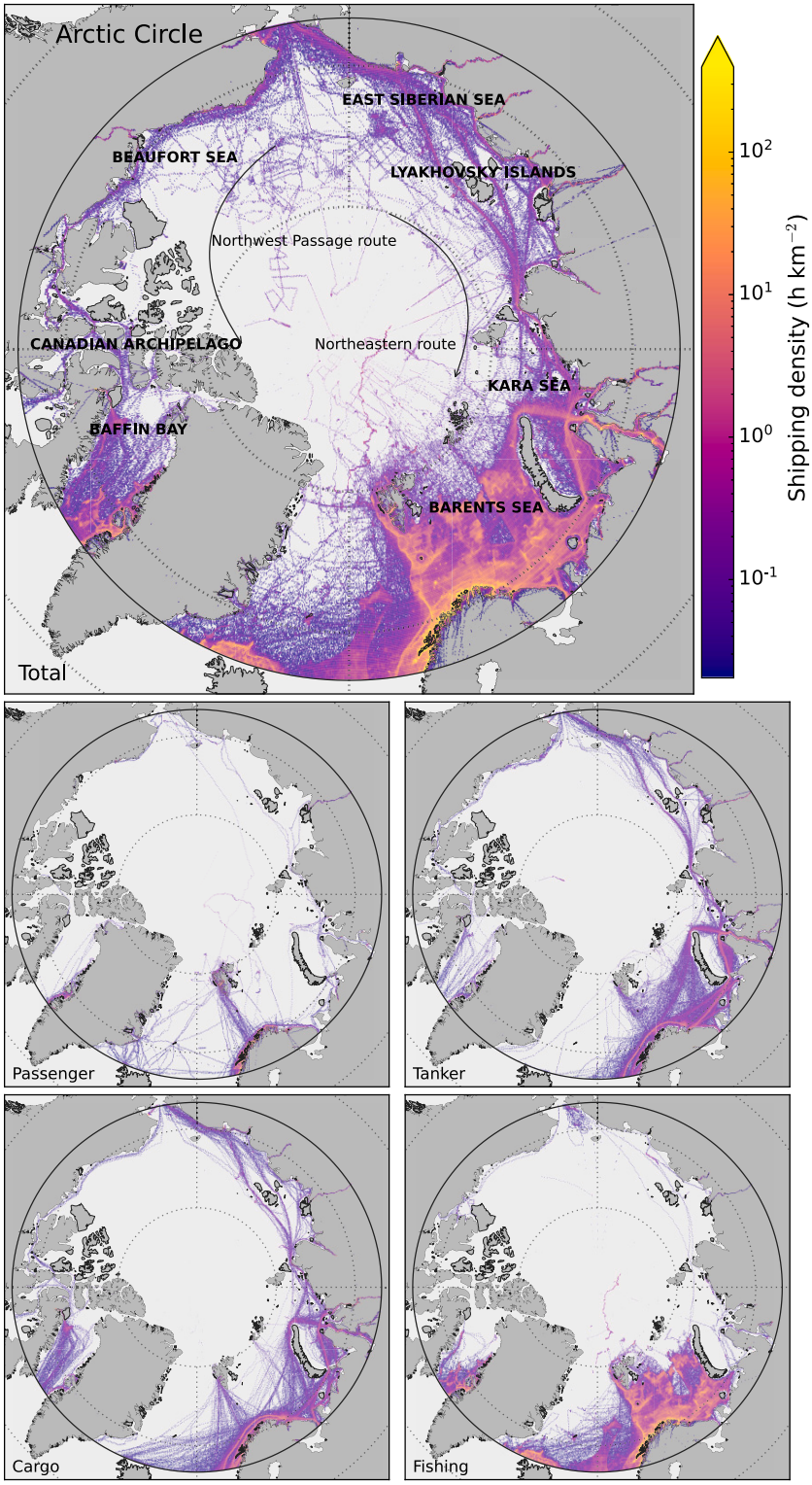

Figure 1. Arctic shipping density between January 2020 and April 2022

Shipping density is computed as the aggregated shipping transit intensity (time spent transiting) over all the vessels, at each 0.1° ×0.1° cell, divided by the cell area. Top panel represents the total shipping traffic, while bottom panels include the traffic for passenger, tanker, cargo, and fishing vessel categories.

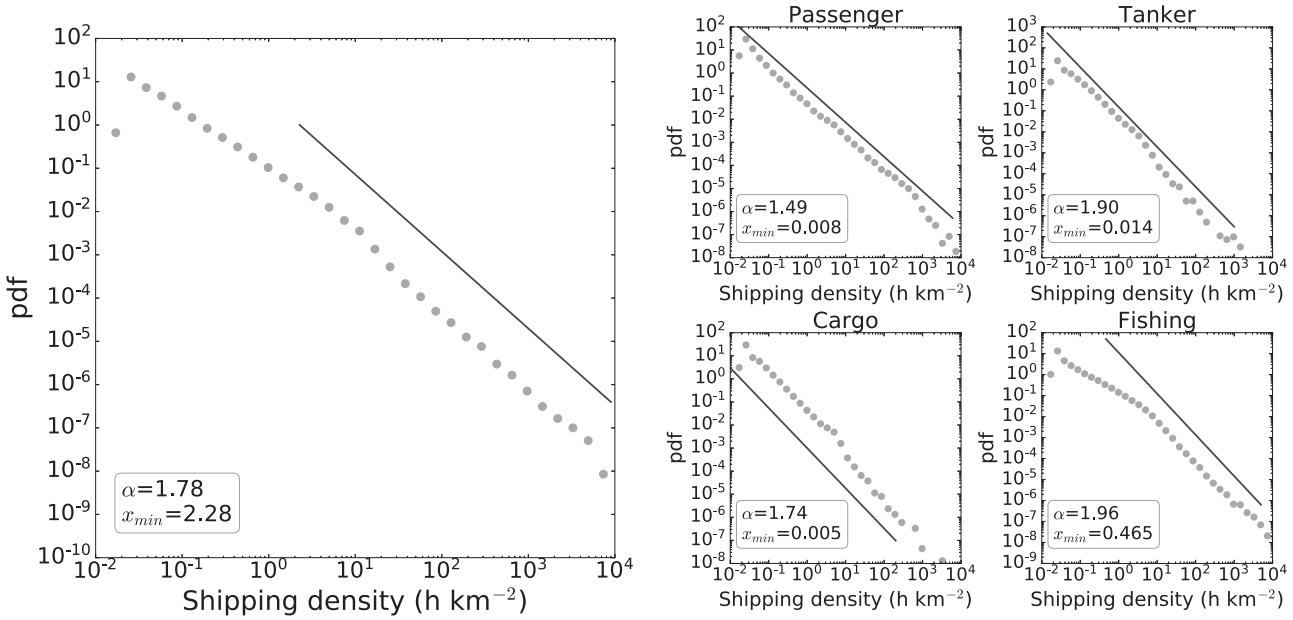

Figure 2. Shipping density distributions for total shipping (left) and each vessel category (right)

These heavy-tailed distributions fit to a power-law distribution $pdf(x) \sim x^{-\alpha}$ for $x > x_{min}$. The slope, obtained from fitting with the Python package *powerlaw*,[20] is represented in the black lines.

highest impact on these two shipping routes is the sea ice area and assessed the correlations between this variable and the shipping width on the selected longitudes of −90° and 150°. We linked the sea ice area in Baffin Bay, Canadian Archipelago, and Beaufort Sea to the Northwest Passage route, and the sea ice area in East Siberian, Kara, and Barents seas to the Northeastern route. We checked the correlations between the shipping width and the sea ice area in these regions, considering only the non-zero shipping widths, obtaining negative values in all the cases (i.e., as expected, an increase in sea ice area led to a decrease in the vessel traffic shipping width). In the case of the Northwest Passage route, the absolute correlation between the vessels' shipping width at −90° longitude and the sea ice area was maximum for the Beaufort Sea

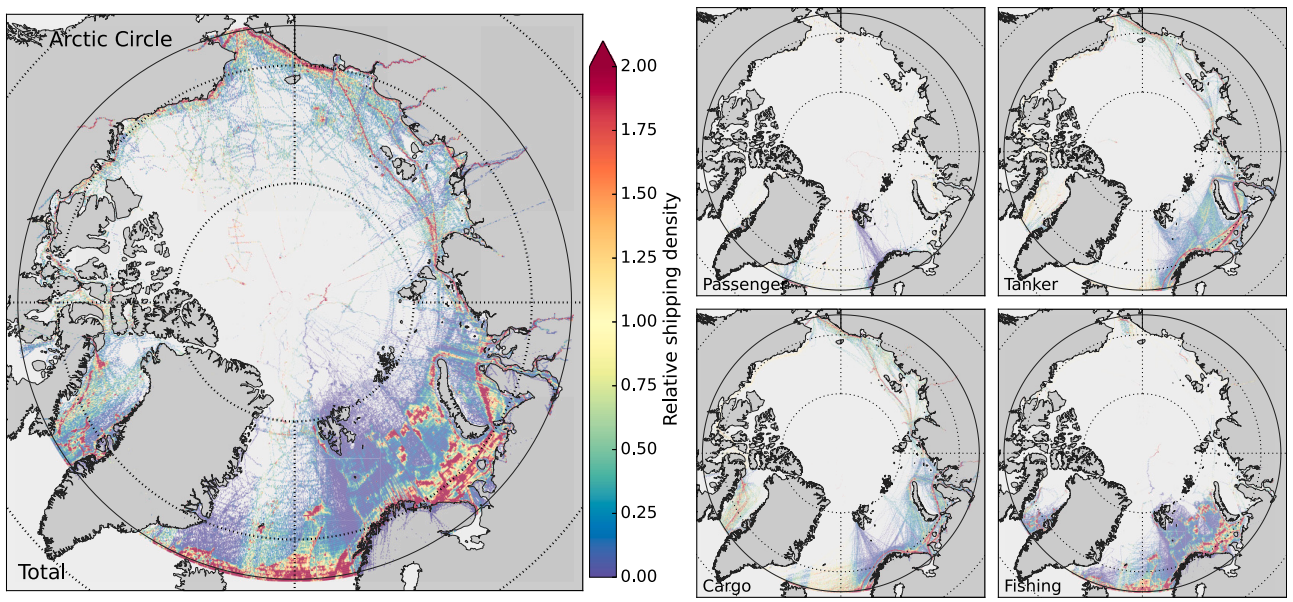

Figure 3. Route detection on shipping traffic

For every cell, given its longitude, we computed the relative shipping density as the shipping density (as represented in Figure 1), divided by the average shipping density for that longitude, computed over cells with non-null density. This highlighted some hotspots at each longitude, which we associate with the shipping routes. Left panel represents the total shipping, while right panels are broken down into vessel categories.

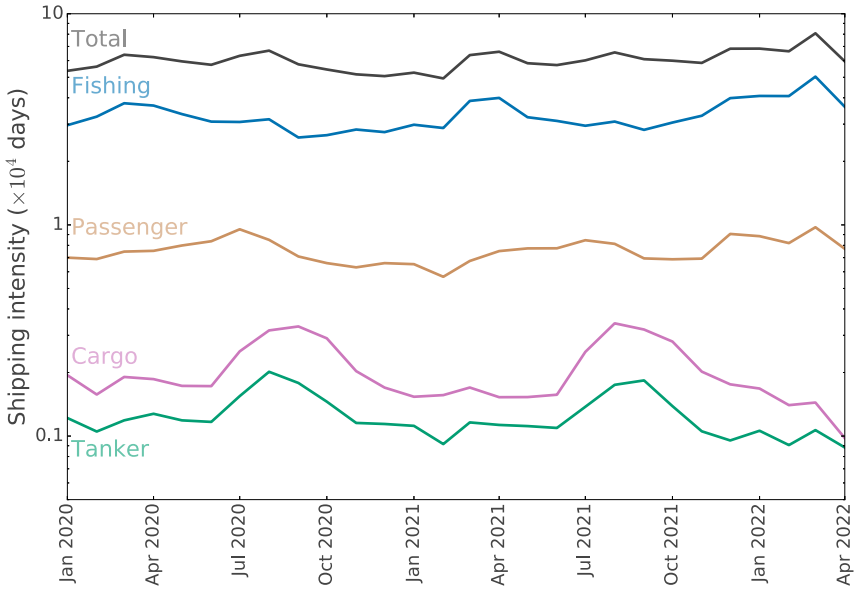

Figure 4. Time evolution of the shipping transit intensity through the Arctic Ocean

The black line represents the total shipping transit intensity, while the colored lines stand for the vessel categories.

($C = -0.90$), with correlations of $C = -0.78$ and $C = -0.72$ for, respectively, the Canadian Archipelago and the Baffin Bay. On the other hand, for the Northeastern route, the absolute correlation between the vessels' shipping width at 150° longitude and the ice area displayed its maximum value for the Kara Sea ($C = -0.842$), showing the correlations of $C = -0.837$ and $C = -0.67$ for, respectively, the East Siberian Sea and the Barents Sea. We focused on the areas with the maximum absolute correlation between the sea ice area and the shipping width for the Northwest Passage and the Northeastern routes, assessing the functional relationship between these variables, finding, as suggested by the negative correlations, that the shipping width was maximum when the sea ice area was minimum (Figure 6, insets), and obtaining an exponential decrease of the shipping width with the sea ice area, with characteristic areas of 1.3×10^5 km^2 and 2.3×10^5 km^2 for the sea ice area in, respectively, the Beaufort Sea and the Kara Sea (Figure 6).

Finally, we quantified the evolution of the Northwest Passage and the Northeastern routes with a previous dataset that described the number of unique vessels observed at each 0.25° × 0.25° grid cell. To warrant the comparability with our dataset, we obtained the vessel shipping width following the same procedure as described earlier, but considering the same grid cell size, that is, cells with 0.25° side. We observed a similar pattern across different years in the case of the Northwest Passage, while the Northeastern route displayed a remarkable reduction in its maximum value on the most recent dataset, together with an extension of the season with non-zero transit (Figure 7).

DISCUSSION

Data availability on the marine environment, for example animal trajectories or threats to the marine life,[21] has been historically limited in contrast to the data describing processes occurring on land. However, a change of paradigm from the community and the scientific funding agencies toward data sharing policies is translated into more frequent marine data releases. In this context, online platforms gathering, cleaning, and standardizing multiple source datasets represent a major benefit to advance marine science.[20,22] Moreover, the availability of servers for online computation brings a shift toward the democratization of not only the data access but also the computational resources to process big data. In this context, we have developed our analysis of the Arctic shipping traffic at no cost using the Ocean Data Connector of HUB Ocean, in a Private Preview Week.

We observed that the shipping density was broadly distributed across the Arctic region, with a few locations with a shipping density that was several orders of magnitude higher than the average shipping densities, revealing hotspots of shipping transit (Figures 1 and 2). We proposed two null models of shipping traffic to understand the observed patterns (see Method details in STAR Methods), obtaining analytically that uniform distributions were associated with one-dimensional traffic, while power-law distributions with exponent $\alpha_{2D} = 3$ represented two-dimensional traffic. Although the observed exponents (Figure 2) were different from these two null models, the models allowed us to understand the variability of these exponents across different vessel categories. Although the exponent was still far from the 2D null model, the highest observed exponent was that of fishing vessels, reflecting the broad 2-dimensional use of space in Barents Sea, together with 1-dimensional transits. The lowest exponent was that of passengers shipping density, expected for more directed trajectories, although heterogeneity in the shipping density (the 1-dimensional null model suggests a flat distribution) may have emerged due to environmental and political factors, such as the weather, the ice distribution, exclusive economic zone boundaries, or oceanic currents. Finally, cargo and tanker vessels' shipping density distributions were described by intermediate exponents ($\alpha_{cargo} = 1.74$, $\alpha_{tanker} = 1.90$), with α_{tanker} being higher, which we link to the higher space occupancy of tanker vessels in the Barents Sea, where cargo vessels displayed more concentrated trajectories (Figure 1).

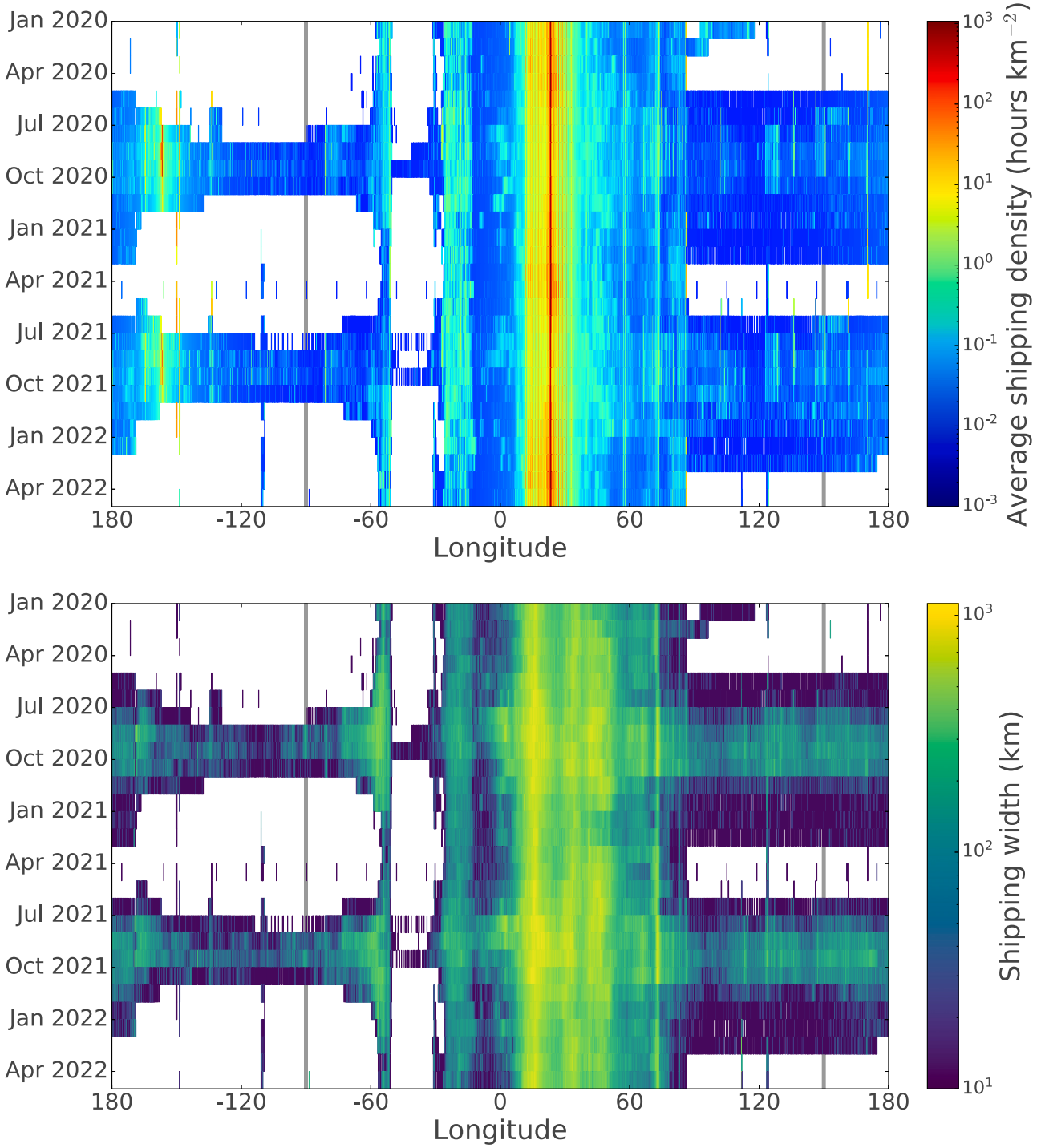

Figure 5. Time evolution of the shipping traffic per longitude

The top panel represents the average shipping density over cells with non-null shipping at each longitude, while the bottom represents the sectional length of these cells. White entries represent the absence of traffic. The gray lines stand for the longitudes that we chose as the most representative for measuring the Northeastern and the Northwest Passage routes being, respectively, 150° and −90°.

Our analysis of the connection between the traffic and the sea ice area revealed maximum absolute (negative) correlations with the sea ice area in regions located far from the locations that we selected as representative for the Northwest Passage and the Northeastern routes. Specifically, for the Northeastern route, we selected the longitude $\lambda_{NE} = 150°$, which crosses the East Siberian Sea, but, although we considered

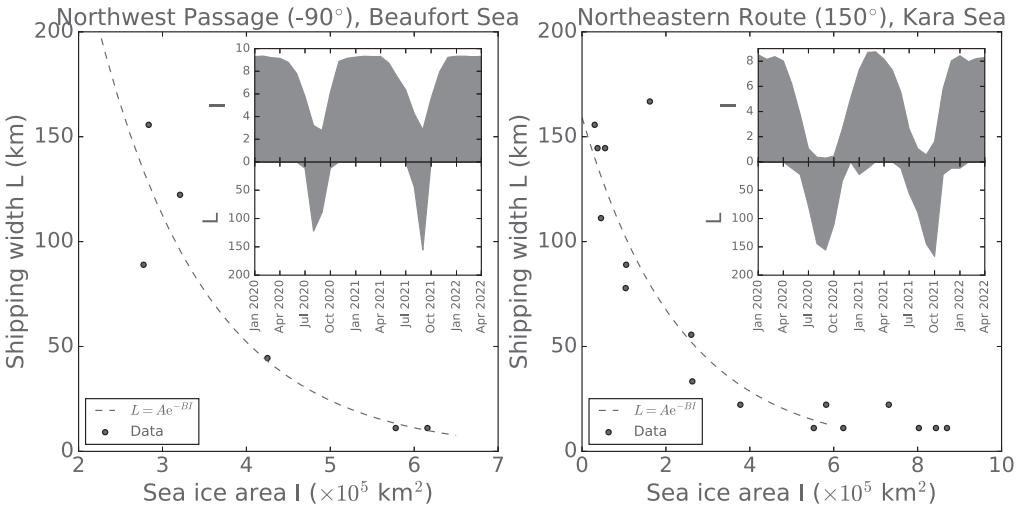

Figure 6. Correlation between shipping width and sea ice area

We selected two specific longitudes that displayed a seasonal behavior: −90° (West, Northwest Passage route) and 150° (East, Northeastern route), computing the shipping width *L* (Figure 5). We computed the Pearson correlation of the shipping width with the non-zero values of the sea ice area in different Arctic seas, obtaining the maximum absolute value of the correlation for the Beaufort Sea (West, $C = -0.90$) and the Kara Sea (East, $C = -0.84$). The main plots represent the shipping width as a function of the sea ice area, while the insets depict their temporal evolution. Points represent data, while the dashed curves are exponentially decreasing fits, $L = Ae^{-BI}$, with $B_{NWP} = 7.68{\times}10^{-6}$ km^{-2} and $B_{NER} = 4.29{\times}10^{-6}$ km^{-2} for, respectively, the Northwest Passage and the Northeastern route.

the sea ice area in that sea, the correlation was higher with the sea ice area in the Kara Sea. Similarly, we selected $\lambda_{NWP} = -90°$ to analyze the shipping width of the Northwest Passage route, crossing the area of the Canadian Archipelago but leading to a higher correlation with the sea ice area in the Beaufort Sea. This suggests the presence of ice bottlenecks where windows of ice-free conditions enable the opening of long-distance routes, such that far locations display a correlation with the sea ice area on these ice bottlenecks.

We quantified the time evolution of shipping traffic on the Northeastern and the Northwest Passage routes with two different datasets; although both datasets reported different variables, our shipping width analysis only considered the presence or absence of shipping on each grid cell, removing possible discrepancies due to the differences across the datasets. This analysis reported an expected seasonal pattern in both routes, displaying a low variability on the Northwest Passage. However, the Northeastern route showed a recent reduction on the maximum shipping width, together with a longer seasonal behavior, i.e., the route was narrower, but used through a longer fraction of the year. The local, regional, and international mobility restrictions to reduce the spread of COVID-19, on the already-called "anthropause,"[23,24] overlapped with most of our analyzed period, implying as well a reduction on factory production rates, and may explain this decrease in the width of the Northeastern route, as a decrease in traffic would lead to vessels following paths that are closer to the optimal, in terms of distance, considering all the geographical and environmental (ice) constraints. In fact, a global analysis revealed a decline of 1.4% on traffic occupancy in the early months of the pandemic, especially in the Northern Hemisphere.[25]

The decline in the extent of sea ice in the Arctic Ocean with rapid Arctic warming represents an opportunity to optimize shipping routes, reducing the transit duration and costs and, therefore, the greenhouse gas emissions. However, this increase in Arctic shipping traffic may be a harbinger of the "blue acceleration"[26] on the Arctic, threatening the marine species that were not previously exposed to shipping hazards,[27] such as ship strikes,[28] underwater noise,[29] or the introduction of invasive species,[30] in addition to other stressors such as the already detected plastic pollution.[31,32] On the other hand, the availability of new shipping routes may represent a human-based negative feedback on global warming, reducing the emissions from vessels due to the use of shorter routes.[33] These potential positive and negative aspects highlight the importance of data analyses to monitor and manage Arctic shipping traffic, conducive to minimize environmental impacts.

Limitations of the study

We acknowledge the limitation of using the total time spent on transit through each grid cell to the estimation of shipping traffic, which could be impacted by the variability on weather conditions or the space-use for non-transit activities such as fishing; nevertheless, this limitation does not affect the shipping width analyses that quantify the seasonal behavior and the correlations with the sea ice extent. We also acknowledge geographical constraints that represent a higher bound to the shipping width, particularly on the Northwest Passage route, although despite them we were able to observe a seasonal trend.

STAR★METHODS

Detailed methods are provided in the online version of this paper and include the following:

- KEY RESOURCES TABLE

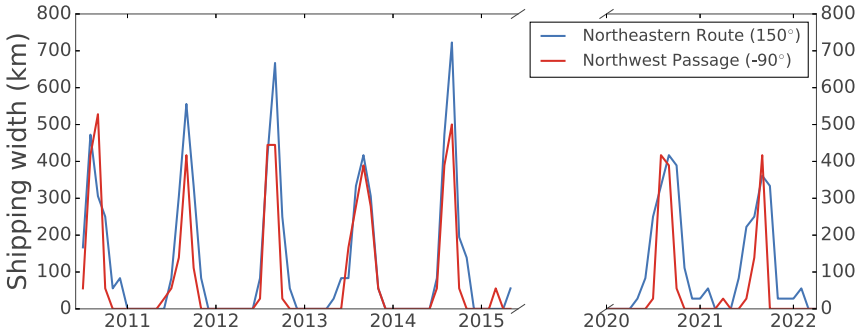

Figure 7. Time evolution of the shipping width at two specific longitudes: −90° (West, Northwest Passage route) and 150° (East, Northeastern route), to characterize the evolution of shipping traffic

The local shipping width is computed as, for each constant longitude and each month, the cross-sectional length of the cells that display non-null shipping traffic. Data between 2010 and 2015 have been extracted from a different database[18] with resolution of 0.25°, number of unique vessels per month. For comparability, this figure includes our analyzed dataset considering grid cells of 0.25° side instead of those of 0.1° side.

ACKNOWLEDGMENTS

J.P.R. was supported by Juan de la Cierva Formacion program (Ref. FJC2019-040622-I) funded by MCIN/AEI/10.13039/501100011033, and by the Vicenç Mut program from Govern de les Illes Balears. J.P.R. received support from Spanish Research Agency MCIN/AEI/10.13039/501100011033 via project MISLAND (PID2020-114324GB-C22).

This research is supported by María de Maeztu Excellence Unit 2023-2027 (Refs. CEX2021-001201-M and CEX2021-001164-M) funded by MCIN/AEI/10.13039/501100011033.

The authors acknowledge the platform HUB Ocean (hubocean.earth) for access to the data and the computational facilities to remotely run all the analyses, through the Ocean Data Connector.

AUTHOR CONTRIBUTIONS

J.P.R.: conceptualization, data curation, formal analysis (leading), software, visualization, and writing – original draft. K.K.: formal analysis and writing – review and editing. C.M.D.: conceptualization and writing – review and editing. V.M.E.: conceptualization, formal analysis (supporting), and writing – original draft.

DECLARATION OF INTERESTS

The authors declare no competing interests.

Received: November 6, 2023
Revised: April 4, 2024
Accepted: June 6, 2024
Published: June 10, 2024

REFERENCES

1. UNCTAD (2021). Review of Maritime Transport (United Nations Publication).
2. Tournadre, J. (2014). Anthropogenic pressure on the open ocean: The growth of ship traffic revealed by altimeter data analysis. Geophys. Res. Lett. *41*, 7924–7932. https://doi.org/10.1002/2014GL061786.
3. Sardain, A., Sardain, E., and Leung, B. (2019). Global forecasts of shipping traffic and biological invasions to 2050. Nat. Sustain. *2*, 274–282. https://doi.org/10.1038/s41893-019-0245-y.
4. Melia, N., Haines, K., and Hawkins, E. (2016). Sea ice decline and 21st century trans-Arctic shipping routes. Geophys. Res. Lett. *43*, 9720–9728. https://doi.org/10.1002/2016GL069315.
5. Müller, M., Knol-Kauffman, M., Jeuring, J., and Palerme, C. (2023). Arctic shipping trends during hazardous weather and sea-ice conditions and the Polar Code's effectiveness. npj Ocean Sustain. *2*, 12. https://doi.org/10.1038/s44183-023-00016-3.
6. Zhang, Y., Meng, Q., and Zhang, L. (2016). Is the Northern Sea Route attractive to shipping companies? some insights from recent ship traffic data. Mar. Pol. *73*, 53–60. https://doi.org/10.1016/j.marpol.2016.07.030.
7. Theocharis, D., Pettit, S., Rodrigues, V.S., and Haider, J. (2018). Arctic shipping: A systematic literature review of comparative studies. J. Transp. Geogr. *69*, 112–128. https://doi.org/10.1016/j.jtrangeo.2018.04.014.
8. Meredith, M., Sommerkorn, M., Cassotta, S., Derksen, C., Ekaykin, A., Hollowed, A., Kofinas, G., Mackintosh, A., Melbourne-Thomas, J., Muelbert, M., et al. (2019). Polar Regions. In IPCC Special Report on the Ocean and Cryosphere in a Changing Climate (IPCC).
9. Comiso, J.C., Meier, W.N., and Gersten, R. (2017). Variability and trends in the Arctic sea ice cover: Results from different techniques. JGR. Oceans *122*, 6883–6900. https://doi.org/10.1002/2017JC012768.
10. Stroeve, J., and Notz, D. (2018). Changing state of Arctic sea ice across all seasons. Environ. Res. Lett. *13*, 103001. https://doi.org/10.1088/1748-9326/aade56.
11. Min, C., Yang, Q., Chen, D., Yang, Y., Zhou, X., Shu, Q., and Liu, J. (2022). The emerging Arctic shipping corridors. Geophys. Res. Lett. *49*, e2022GL099157. https://doi.org/10.1029/2022GL099157.
12. Cao, Y., Liang, S., Sun, L., Liu, J., Cheng, X., Wang, D., Chen, Y., Yu, M., and Feng, K. (2022). Trans-Arctic shipping routes expanding faster than the model projections. Glob. Environ. Change *73*, 102488. https://doi.org/10.1016/j.gloenvcha.2022.102488.
13. Kroodsma, D.A., Mayorga, J., Hochberg, T., Miller, N.A., Boerder, K., Ferretti, F., Wilson, A., Bergman, B., White, T.D., Block, B.A., et al. (2018). Tracking the global footprint of fisheries. Science *359*, 904–908. https://doi.org/10.1126/science.aao5646.
14. Rodríguez, J.P., Fernández-Gracia, J., Duarte, C.M., Irigoien, X., and Eguíluz, V.M. (2021). The global network of ports supporting high seas fishing. Sci. Adv. *7*, eabe3470. https://doi.org/10.1126/sciadv.abe3470.
15. Frawley, T.H., Muhling, B., Welch, H., Seto, K.L., Chang, S.-K., Blaha, F., Hanich, Q., Jung, M., Hazen, E.L., Jacox, M.G., and Brodie, S. (2022). Clustering of disaggregated fisheries data reveals functional longline fleets across the Pacific. One Earth *5*, 1002–1018. https://doi.org/10.1016/j.oneear.2022.08.004.
16. Queiroz, N., Humphries, N.E., Couto, A., Vedor, M., Da Costa, I., Sequeira, A.M.M., Mucientes, G., Santos, A.M., Abascal, F.J., Abercrombie, D.L., et al. (2019). Global spatial risk assessment of sharks under the footprint of fisheries. Nature *572*, 461–466. https://doi.org/10.1038/s41586-019-1444-4.
17. Halliday, W.D., Le Baron, N., Citta, J.J., Dawson, J., Doniol-Valcroze, T., Ferguson, M., Ferguson, S.H., Fortune, S., Harwood, L.A., Heide-Jørgensen, M.P., et al. (2022). Overlap between bowhead whales (Balaena mysticetus) and vessel traffic in the North American Arctic and implications for conservation and management. Biol. Conserv. *276*, 109820. https://doi.org/10.1016/j.biocon.2022.109820.
18. Eguíluz, V.M., Fernández-Gracia, J., Irigoien, X., and Duarte, C.M. (2016). A quantitative assessment of Arctic shipping in 2010–2014. Sci. Rep. *6*, 30682. https://doi.org/10.1038/srep30682.
19. Silber, G.K., and Adams, J.D. (2019). Vessel operations in the Arctic, 2015–2017. Front. Mar. Sci. *6*, 573. https://doi.org/10.3389/fmars.2019.00573.
20. Tanhua, T., Pouliquen, S., Hausman, J., O'Brien, K., Bricher, P., De Bruin, T., Buck, J.J.H., Burger, E.F., Carval, T., Casey, K.S., et al. (2019). Ocean FAIR data services. Front. Mar. Sci. *6*, 440. https://doi.org/10.3389/fmars.2019.00440.
21. Sequeira, A.M.M., Hays, G.C., Sims, D.W., Eguíluz, V.M., Rodríguez, J.P., Heupel, M.R., Harcourt, R., Calich, H., Queiroz, N., Costa, D.P., et al. (2019). Overhauling ocean spatial planning to improve marine megafauna conservation. Front. Mar. Sci. *6*, 639. https://doi.org/10.3389/fmars.2019.00639.
22. Buck, J.J.H., Bainbridge, S.J., Burger, E.F., Kraberg, A.C., Casari, M., Casey, K.S., Darroch, L., Rio, J.D., Metfies, K., Delory, E., et al. (2019). Ocean data product integration through innovation-the next level of data interoperability. Front. Mar. Sci. *6*, 32. https://doi.org/10.3389/fmars.2019.00032.
23. Rutz, C., Loretto, M.-C., Bates, A.E., Davidson, S.C., Duarte, C.M., Jetz, W., Johnson, M., Kato, A., Kays, R., Mueller, T., et al. (2020). COVID-19 lockdown allows researchers to quantify the effects of human activity on wildlife. Nat. Ecol. Evol. *4*, 1156–1159. https://doi.org/10.1038/s41559-020-1237-z.
24. Bates, A.E., Primack, R.B., Biggar, B.S., Bird, T.J., Clinton, M.E., Command, R.J., Richards, C., Shellard, M., Geraldi, N.R., Vergara, V., et al. (2021). Global COVID-19 lockdown highlights humans as both threats and custodians of the environment. Biol. Cons. *263*, 109175. https://doi.org/10.1016/j.biocon.2021.109175.
25. March, D., Metcalfe, K., Tintoré, J., and Godley, B.J. (2021). Tracking the global reduction of marine traffic during the COVID-19 pandemic. Nat. Commun. *12*, 2415. https://doi.org/10.1038/s41467-021-22317-1.
26. Jouffray, J.-B., Blasiak, R., Norström, A.V., Österblom, H., and Nyström, M. (2020). The blue acceleration: the trajectory of human expansion into the ocean. One Earth *2*, 43–54. https://doi.org/10.1016/j.oneear.2019.12.016.
27. Burek, K.A., Gulland, F.M.D., and O'Hara, T.M. (2008). Effects of climate change on Arctic marine mammal health. Ecol. Appl. *18*, S126–S134. https://doi.org/10.1890/06-0553.1.
28. Reeves, R., Rosa, C., George, J., Sheffield, G., and Moore, M. (2012). Implications of Arctic industrial growth and strategies to mitigate future vessel and fishing gear impacts on bowhead whales. Mar. Pol. *36*, 454–462. https://doi.org/10.1016/j.marpol.2011.08.005.
29. Tervo, O.M., Blackwell, S.B., Ditlevsen, S., Garde, E., Hansen, R.G., Samson, A.L., Conrad, A.S., and Heide-Jørgensen, M.P. (2023). Stuck in a corner: Anthropogenic noise threatens narwhals in their once pristine Arctic habitat. Sci. Adv. *9*, eade0440. https://doi.org/10.1126/sciadv.ade0440.
30. Miller, A.W., and Ruiz, G.M. (2014). Arctic shipping and marine invaders. Nat. Clim. Change *4*, 413–416. https://doi.org/10.1038/nclimate2244.
31. Cózar, A., Martí, E., Duarte, C.M., García-de Lomas, J., Van Sebille, E., Ballatore, T.J., Eguíluz, V.M., González-Gordillo, J.I., Pedrotti, M.L., Echevarría, F., et al. (2017). The Arctic Ocean as a dead end for floating plastics in the North Atlantic branch of the Thermohaline Circulation. Sci. Adv. *3*, e1600582. https://doi.org/10.1126/sciadv.1600582.
32. Peeken, I., Primpke, S., Beyer, B., Gütermann, J., Katlein, C., Krumpen, T., Bergmann, M., Hehemann, L., and Gerdts, G. (2018). Arctic sea ice is an important temporal sink and means of transport for microplastic. Nat. Commun. *9*, 1505. https://doi.org/10.1038/s41467-018-03825-5.
33. Browse, J., Carslaw, K.S., Schmidt, A., and Corbett, J.J. (2013). Impact of future Arctic shipping on high-latitude black carbon deposition. Geophys. Res. Lett. *40*, 4459–4463. https://doi.org/10.1002/grl.50876.
34. Alstott, J., Bullmore, E., and Plenz, D. (2014). powerlaw: A Python package for analysis of heavy-tailed distributions. PLoS One *9*, e85777. https://doi.org/10.1371/journal.pone.0085777.
35. Fetterer, F., Knowles, K., Meier, W.N., Savoie, M.M., and Windnagel, A.K. (2017). Sea Ice Index. version 3. https://nsidc.org/data/G02135/versions/3.

STAR★METHODS

KEY RESOURCES TABLE

REAGENT or RESOURCE	SOURCE	IDENTIFIER
Deposited data		
Analyzed data	This paper	Database: https://github.com/jorgeprodriguezg/Arctic-shipping/tree/main/data
Software and algorithms		
powerlaw package	Alstott et al.[34]	https://pypi.org/project/powerlaw/
Analysis and figure generation	This paper	https://github.com/jorgeprodriguezg/Arctic-shipping/

RESOURCE AVAILABILITY

Lead contact

Further information and requests for resources and reagents should be directed to and will be fulfilled by the Lead Contact, Dr. Jorge P. Rodríguez (jorge@ifisc.uib-csic.es).

Materials availability

This study did not generate new unique materials.

Data and code availability

- Data. The data sets supporting the results of this article is(are) publicly available in the 'Arctic shipping' repository, https://github.com/jorgeprodriguezg/Arctic-shipping/tree/main/data.
- Code. The Jupyter notebooks used for the analysis and generating the figures are publicly available in the 'Arctic shipping' repository https://github.com/jorgeprodriguezg/Arctic-shipping.
- Any additional information required to reanalyze the data reported in this paper is available from the lead contact upon request.

METHOD DETAILS

Shipping traffic

The use of space by ships transiting the Arctic Ocean was inferred from the Automatic Identification System (AIS) data. AIS is a system introduced for maritime safety that provides, among different data variables, the speed, latitude and longitude of the vessels using the system. The Ocean Data Connector aggregated AIS tracking data at a monthly resolution and reported the total number of hours spent on transit through each grid cell by all the vessels that visited it, which we named shipping transit intensity. The monthly transiting time was available from January 2020 to April 2022, and it specified four vessel categories (cargo, fishing, passenger and tanker). For our analysis, we introduced a global grid of 0.1°×0.1° resolution to measure the shipping transit intensity and selected latitudes higher than the Arctic Circle (66.6°, Figure 1).

The time evolution of the area covered by the shipping routes was complemented with the dataset used for a previous assessment of the Arctic shipping traffic,[18] to provide a comparison of the Ocean Data Connector dataset and illustrate the time evolution of the shipping traffic in the Arctic Ocean. This previous dataset reported the monthly number of unique vessels detected by the AIS system in each 0.25°×0.25° grid cell, between July 2010 and May 2015.

Shipping density

For each grid cell, we obtained the shipping density by dividing the shipping transit intensity (time spent transiting) by the cell area A:

$$A = R^2\left(\sin\frac{\pi(\phi+\Delta\phi)}{180} - \sin\frac{\pi\phi}{180}\right)\frac{\Delta\lambda\pi}{180} \quad \text{(Equation 1)}$$

where $R = 6371$ km is the Earth radius, ϕ is the latitude in degrees, and $\Delta\lambda$ and $\Delta\phi$ are, respectively, the longitudinal and latitudinal sides of the cell in degrees.

Average shipping density per longitude

We compute the average shipping density per longitude as the sum of the total shipping transit intensities through cells with the same longitude, divided by the area of those cells with a non-zero shipping transit intensity, following Equation 1 For the time evolution of this value, at each time step we only consider the cells with non-zero shipping transit intensity on that specific period.

Shipping width per 0.1° longitude

We consider all the grid cells in the Arctic region with a specific longitude λ, and compute the time evolution of the number of cells $N(\lambda, t)$ that displayed a non-zero shipping transit intensity. We computed the shipping width $W(\lambda, t)$ as the length of the latitudinal cross-section of these cells:

$$W(\lambda, t) = RN(\lambda, t)\frac{\Delta\phi\pi}{180} \quad \text{(Equation 2)}$$

Sea ice cover

Sea ice area was obtained from the Sea Ice Index, provided by the National Snow and Ice Data Center (United States).[35] This dataset reported the monthly evolution of the sea ice area in the Northern Hemisphere, as well as specific subregions of the Arctic, where we considered the Canadian Archipelago Area, the Baffin Bay and the Beaufort Sea for the Northwest Passage route, while we considered the East Siberian Sea, the Kara Sea and the Barents Sea for the Northeastern route.

Null model of shipping density

We propose a null model of transit between geographical locations to understand the differences between the shipping distributions for different vessel types, and we apply it to one- and two-dimensional systems. In a one-dimensional system, ships can move on a line, modifying their coordinate x and always with a constant and positive speed $v = \frac{dx}{dt}$. We consider a destination located at $x = 1$, and the origins distributed uniformly in the interval $[0, 1)$, with vessels departing randomly from any of these origins. We aim at computing the distribution of the shipping density across different locations. The total transit intensity (sum of the transit time over all the vessels) between x and $x + dx$ will be given by the number of vessels that crossed that region, that is, Nx, with N being the total number of vessels, and x being the probability that a vessel departs from a location lower than x, times dx/v (i.e., the transit intensity of one vessel), implying that the shipping density ρ_{1d}, i.e. the transit intensity per unit length, is

$$\rho_{1d}(x) = \frac{Nx}{v} \quad \text{(Equation 3)}$$

Thus, the cumulative distribution function (CDF) of the shipping density ρ_{1d} is the length of the segment with locations that have a shipping density time lower than ρ_{1d}. This length is x in Equation 3, leading to

$$\mathrm{CDF}(\rho_{1d}) = \frac{\rho_{1d}v}{N} \quad \text{(Equation 4)}$$

with $\rho_{1d} \in \left(0, \frac{N}{v}\right]$. Taking the derivative of the cumulative distribution function, this leads to a uniform probability density function (pdf)

$$\mathrm{pdf}(\rho_{1d}) = \frac{v}{N} \quad \text{(Equation 5)}$$

In two dimensions, we consider that the origin is located at the origin of coordinates, while the destinations are located uniformly at a distance from the origin $R = 1$, and the vessels transit with ballistic motion at speed v from the origin towards a randomly chosen destination. In this case, considering the polar coordinates r and ϕ, we compute the shipping transit intensity of a vessel that crosses a region at distance r from the origin of size $dr \times d\phi$. Analogously to the one-dimensional system, the shipping transit intensity of a vessel is dr/v. Additionally, the number of vessels that transit this region is $Nd\phi/(2\pi)$, leading to a total shipping transit intensity of $\frac{Ndrd\phi}{2\pi v}$. However, if we consider cells of size $dr \times d\phi$, these cells will be larger for higher r, such that the number of vessels on them does not represent the shipping density. To solve this, we consider uniform cells of size $dxdy$, with $drd\phi = \frac{dxdy}{r}$. Thus, the shipping density, obtained as the shipping transit intensity per unit area, ρ_{2d}:

$$\rho_{2d}(r, \phi) = \frac{N}{2\pi r v} \quad \text{(Equation 6)}$$

which, due to the symmetry of the system, does not depend on ϕ. In this case, the cumulative distribution function will be the fraction of area with density lower than ρ. This area will be $\pi R^2 - \pi r^2$, and considering from (6) $r = \frac{N}{2\pi\rho_{2d}v}$, we obtain

$$\mathrm{CDF}(\rho_{2d}) = 1 - \frac{N^2}{4\pi^2\rho_{2d}^2 v^2} \quad \text{(Equation 7)}$$

with $\rho_{2d} \in \left[\frac{N}{2\pi v}, \infty\right)$. Taking the derivative of the cumulative distribution function, we obtain the probability density function, described by a power-law

$$\mathrm{pdf}(\rho_{2d}) = \frac{N^2 \rho_{2d}^{-3}}{2\pi^2 v^2} \quad \text{(Equation 8)}$$

QUANTIFICATION AND STATISTICAL ANALYSIS

The Python *powerlaw*[34] package was used to estimate the power-law exponents of the distributions shown in Figure 2.